IEEE Photonics Journal
An IEEE Photonics Society Publication

Giant Birefringence of Periodic Dielectric Waveguides

Volume 3, Number 3, June 2011

Wenfu Zhang
Jihong Liu
Wei-Ping Huang, Senior Member, IEEE
Wei Zhao

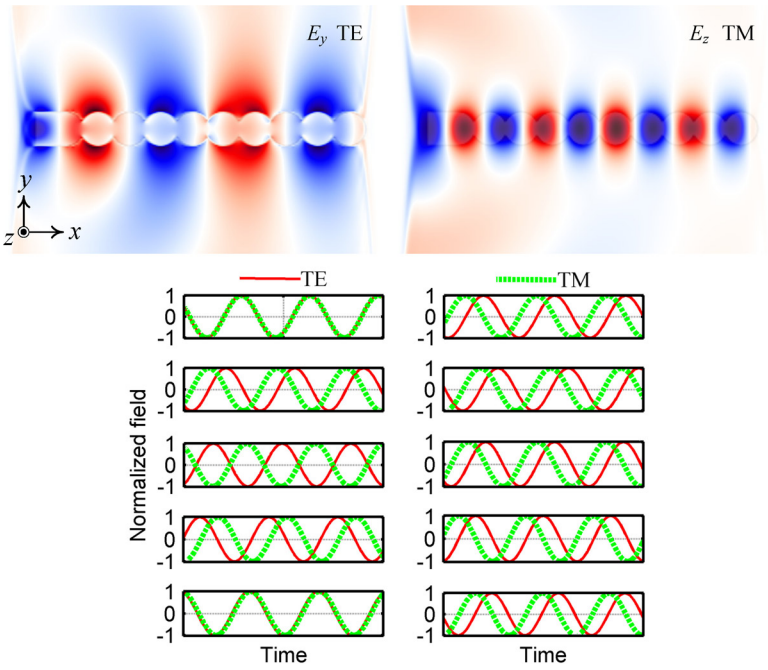

DOI: 10.1109/JPHOT.2011.2154319
1943-0655/$26.00 ©2011 IEEE

Giant Birefringence of Periodic Dielectric Waveguides

Wenfu Zhang,[1,2] **Jihong Liu,**[3]
Wei-Ping Huang,[4] ***Senior Member, IEEE*, and Wei Zhao**[1]

[1]State Key Laboratory of Transient Optics and Photonics, Xi'an Institute of Optics and Precision Mechanics, Chinese Academy of Sciences, Xi'an 710119, China
[2]Graduate School of the Chinese Academy of Sciences, Beijing 100049, China
[3]Department of Electronic and Information Engineering, Xi'an University of Posts and Telecommunications, Xi'an 710061, China
[4]Department of Electrical and Computer Engineering, McMaster University, Hamilton, ON L8S 4K1, Canada

DOI: 10.1109/JPHOT.2011.2154319

Manuscript received May 2, 2011; revised May 6, 2011; accepted May 6, 2011. Date of publication May 12, 2011; date of current version June 3, 2011. This work was supported by the Chinese Academy of Sciences/State Administration of Foreign Expert Affairs (CAS/SAFEA) International Partnership Program for Creative Research Teams. Corresponding author: W. Zhang (e-mail: wfu.zhang@gmail.com; wfuzhang@opt.cas.cn).

Abstract: The giant $(\Delta n > 1.5)$ and broadband achromatic birefringence is realized by periodic dielectric waveguides (PDWs), which benefit from low loss transmission, compact size, and simple structure. Based on the PDW, ultrabroadband achromatic (> 100 nm), low-order ultracompact $(< \lambda)$, and ultrahigh-order (500th order) wave plates are designed successfully.

Index Terms: Subwavelength structures, nanostructures, photonic crystals, waveguide devices, waveguides.

1. Introduction

Birefringence [1]–[7], which describes the refractive index difference (Δn) of different polarizations, plays an important role in modern optical devices, such as wave plates (WPs), optical filters, modulators, sensors, etc. There are two kinds of birefringence: One is microscopic anisotropy induced (natural birefringence), and the other is macroscopic anisotropy induced (artificial birefringence) [4]. For the designable characteristic, artificial birefringence has attracted a lot of attention and has recently been shown in different structures [3]–[7]. As shown in Table 1, some artificial structures, (e.g., metamaterials (MMs) [3], plasmonic nanoslit array (PNA) [4], multislotted dielectric waveguides (MSDWs) [5], and photonic crystals (PhCs) [6], [7]) can achieve giant birefringence $(\Delta n > 1)$. MMs have ultrahigh birefringence for possessing refractive indices of two orthogonal polarization lights in opposite signs. However, the application of this ultrahigh birefringence is limited by a narrow operating band induced by the high dispersion of MMs [3] and the difficulty of fabricating in a short wavelength. The birefringence in the PNA is large if the nanoslit is narrow. However, the transmission efficiency is relatively low under this condition [4]. PhCs have the benefits of flexibility in structure design and facility in birefringence tuning [7]. The drawback is the beam divergence in the nonwaveguiding structure [8]. Recently, we have introduced the self-collimating effect of PhC to deal with beam divergence [8], but the loss is high when the PhC has an ultralarge size in the direction of wave propagation. Although MSDW proposed in [5] is prominent in many aspects, such as low loss, all-dielectric waveguide structure, and achromatic characteristics,

TABLE 1

Giant artificial birefringence of different structures

	Multilayer film	Nanowire	MM	PNA	MSDW	PhC
Δn	~ 0.3	~ 0.8	~ 3.2	2.7	$\sim 1.0^{\dagger}$	0.938
Achromatic	-	-	No	No	-	Yes
Loss	Low	-	High	High	Low	Low
Reference	[1]	[2]	[3]	[4]	[5]	[6]
†This is the phase birefringence						

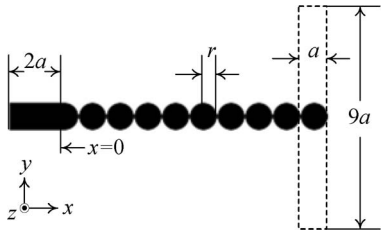

Fig. 1. Top view of the structure of PDW. The light propagates along *x* direction.

the effective indices difference between two orthogonal polarizations is not very high (∼1), and the high-order modes may exist in the waveguide.

In addition to the structures mentioned above, the periodic dielectric waveguide (PDW) [9]–[24], which is also known as nanopillar periodic waveguide [12]–[16] or coupled periodic waveguide [17], [18], is another artificial periodic structure attracting a lot of research interest. It can be seen as a simple form of PhC waveguide and has potential applications in waveguides [9]–[15], lasing [16], slow light [18], [19], high Q cavities [20], splitters [21]–[24], etc. In this paper, the birefringence of PDWs with high index dielectric rods in air is studied thoroughly, and a large effective index difference (> 1.5, which is the largest value in all dielectric structure to our knowledge) is achieved. Although the birefringence is not as large as those of PNAs and MMs, the PDW benefits from lower transmission loss (compared with PNAs) and wider operating bandwidth (compared with MMs). Besides ultracompact low-order WPs, broadband (> 100 nm) achromatic low-order WPs and compact high-order WPs based on formed birefringence are designed. Comparing with the PhC WPs (see [8] and references therein), the WPs based on PDW have larger achromatic bandwidth, more compact size and simpler structure.

2. Birefringence of PDWs

Fig. 1 shows the physical structure of PDW with high index dielectric rods in air. It is a 2-D structure with dielectric rods having infinite length in the *z* direction. The band structures of PDWs with dielectric rods having different permittivity (ε) and radius (r) are calculated by a plane wave method (PWM) [25] with a supercell of $1 \times 9a$, where *a* is the lattice constant, and two of them are shown in Fig. 2(a) $(r = 0.45a, \varepsilon = 8.9)$ and (b) $(r = 0.65a, \varepsilon = 8.9)$. From the band structures, we can see that, at the given frequency ranges, i.e., between the horizontal dot lines in Fig. 2, the PDWs have one transverse electric (TE) and one transverse magnetic (TM) mode with different effective indices (ck/ω).

Fig. 3 shows the effective index difference $(\Delta n = n_{TM} - n_{TE})$ of PDWs with different parameters. All the curves are calculated in the band regions in which only one TE and one TM mode exist. From the figures, we can see that 1) large Δn can be realized in PDWs. The higher the permittivity of dielectric rods is, the larger Δn is. When the permittivity is 12.96 (GaAs), the effective difference can be larger than 1.5. 2) When the radius of the rod is relatively small (such as $r = 0.45a$ or

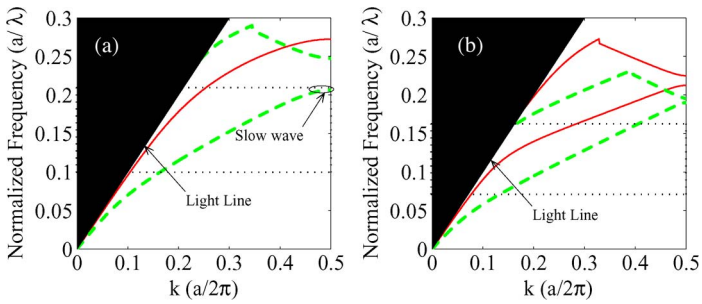

Fig. 2. (a) Dispersion curve of PDW with $r = 0.45a$ and $\varepsilon = 8.9$. (b) Dispersion curve of PDW with $r = 0.65a$ and $\varepsilon = 8.9$. TE guiding modes are plotted as red solid curves and green dashed lines are for TM.

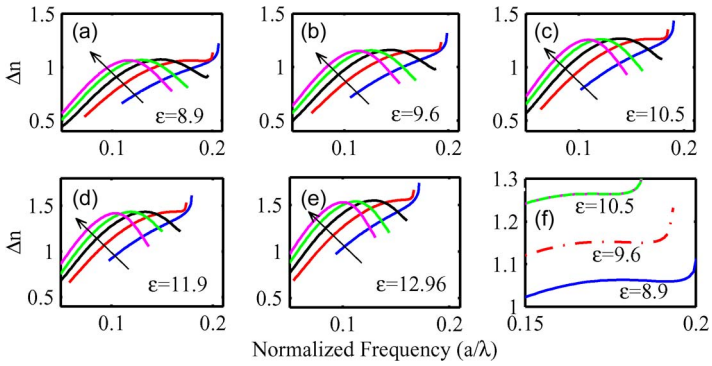

Fig. 3. Birefringence (Δn) of PDWs with different parameters for (a) $\varepsilon = 8.9$, (b) $\varepsilon = 9.5$, (c) $\varepsilon = 10.5$, (d) $\varepsilon = 11.9$, and (e) $\varepsilon = 12.96$, respectively. In (a)–(e), following the direction of the arrows, the curves represent the birefringence of PDWs with different r of $0.45a$, $0.50a$, $0.55a$, $0.60a$, and $0.65a$, respectively. (f) Zoom-in picture of Δn. The radius of the dielectric rod is $r = 0.50a$.

$r = 0.50a$), the values of Δn at the upper edge change rapidly for the TM modes reach the slow wave region [see Fig. 2(a)]. It is useful for applications that need large polarization dispersion such as optical depolarizing. The largest value of Δn locates at this narrow frequency band. 3) Except for the slow wave region, the largest value of Δn in PDWs with different radii are almost equal if the permittivities are the same. 4) There are *flat* sections $(d\Delta n/d\omega \sim 0)$ when $r \geq 0.50a$, especially when r equals $0.5a$. From the zooming in curves shown in Fig. 3(f), we can see that the effective index differences are almost equal in a large frequency range. For example, Δn locates in the range of 1.0595–1.0635 at the frequency band of 0.169–0.196 a/λ for $\varepsilon = 8.9$, 1.1505–1.1530 at 0.167–0.188 a/λ for $\varepsilon = 9.6$, and 1.264–1.265 at 0.165–0.178 a/λ for $\varepsilon = 10.5$. These reveal that PDW has achromatic birefringence in a wide frequency band.

3. Phase Difference of TE and TM Polarizations for PDWs

Although the achromatic birefringence is important for some applications, the achromatic phase difference between two polarizations in broadband is more attractive for WP applications. The phase difference $(\Delta\varphi)$ between TE and TM polarization after transmitting a distance of L can be expressed as $\Delta\varphi = 2\pi\Delta nL/\lambda$. Fig. 4 shows the phase differences of PDWs with different parameters at the situation of $L = 4a$.

From the expression of phase difference, $\Delta\varphi$ is not only related to Δn but to L and λ as well. Therefore, the curves of $\Delta\varphi$ are quite different from that of Δn. From Fig. 4, the achromatic phase differences appear when the values of r are equal to or larger than $0.55a$. When $r = 0.55a$, there are largest bandwidths of achromatic phase differences for PDWs with different dielectric rods,

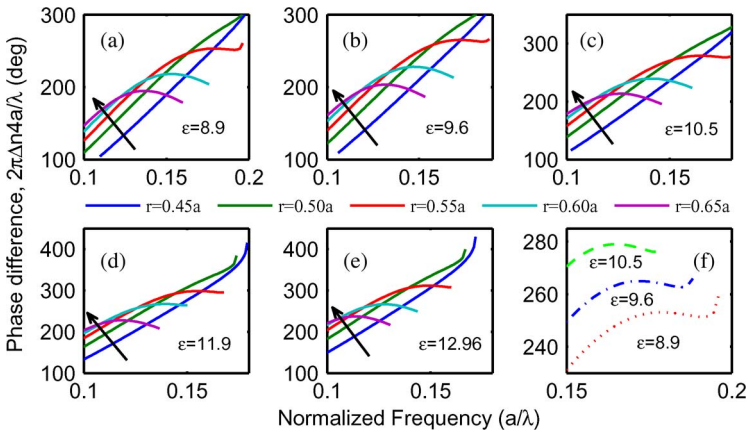

Fig. 4. Phase differences $(\Delta\varphi)$ of PDWs with different parameters for (a) $\varepsilon = 8.9$, (b) $\varepsilon = 9.5$, (c) $\varepsilon = 10.5$, (d) $\varepsilon = 11.9$, and (e) $\varepsilon = 12.96$, respectively. In (a)–(e), following the direction of the arrows, the curves represent the phase differences with different r of 0.45a, 0.50a, 0.55a, 0.60a, and 0.65a, respectively. (f) Zoom-in picture of $\Delta\varphi$. The radius of the dielectric rod is $r = 0.55a$. The length of the PDW is supposed as $L = 4a$.

which can be seen in Fig. 4(f). The critical value for achromatic phase differences $(r = 0.55a)$ is different from that of the achromatic birefringence $(r = 0.50a)$.

Based on the PDW, ultracompact WP is designed. For the giant birefringence of PDWs, a 2π phase difference $(\Delta\varphi = 2\pi)$ can be realized by a short transmission distance that is less than λ $(L < \lambda)$ when Δn is large enough. Taking $r = 0.55a$, $\varepsilon = 12.96$ as an example, if $\omega = 0.145\ a/\lambda$, a 2π phase difference is introduced by $L = 4.63a$, which is shorter than $\lambda = 6.9a$ ($\Delta n = 1.488$ at this frequency).

The 2-D finite-difference time domain (FDTD) simulation method [26] is used to verify the phase characteristics of the WPs designed above. The mesh size and time step are $\Delta x = \Delta y = 0.05a$ and $\Delta t = 0.5/(c\sqrt{(1/\Delta x)^2 + (1/\Delta y)^2})$. The simulated structure $(r = 0.55a, \varepsilon = 12.96)$ is similar to Fig. 1. Two upper figures in Fig. 5 are snapshots of the electric field E_y for TE and E_z for TM, respectively. The continuous wave (CW) source with the frequency of 0.145 a/λ is launched at $x = -a$ in the adjacent dielectric waveguide. A set of point monitors are inserted in the center of the propagation beam in the y direction, where the dashed line in the top of Fig. 5, at different places along the x direction, to detect the electric field (E_y for TE and E_z for TM) at different times. In Fig. 5(a)–(f), normalized E_y (TE) and E_z (TM) are plotted. The phase of E_y and E_z at $x = 3.4a$ is identical [as shown in Fig. 5(a)]. After transmitting to $x = 4.5a$, as shown in Fig. 5(b), the phase difference between TE and TM is $\pi/2$. Furthermore, the phase differences are π at $x = 5.55a$ [see Fig. 5(c)], $3\pi/2$ at $x = 6.55a$ [see Fig. 5(d)], and 2π at $x = 8.0a$ [see Fig. 5(e)]. These results certify that the PDW with length of 4.5a and 5.55a (the real lengths are about 0.6525λ and 0.80475λ, respectively) can be served as the first-order quarter and half WP at frequency of 0.145 a/λ, respectively. The phase difference of 2π is introduced by the distance of 4.6a, and this is in good agreement with the theoretical value of 4.63a calculated above. To verify the broadband achromatic property of the phase difference, CW sources with different frequencies are launched into the PDW $(r = 0.55a, \varepsilon = 12.96)$, and the detector is located at $x = 4.5a$ unchanged. Fig. 5(f)–(j) show that the phase differences are fixed at $\pi/2$ in frequency range of 0.140–0.150 a/λ. The frequency range [(1498–1605 nm)] almost covers the whole telecommunication band $(C + L + S)$ if taking the central frequency 0.145 a/λ as 1550 nm $(a = 224.8$ nm$)$.

4. Birefringence and Phase Difference of PDWs With Material Dispersion

In practice, material dispersion can still affect the birefringence of the PDW since the indices are different at different wavelength. Here, we take Silicon (Si) as the high index material to evaluate the

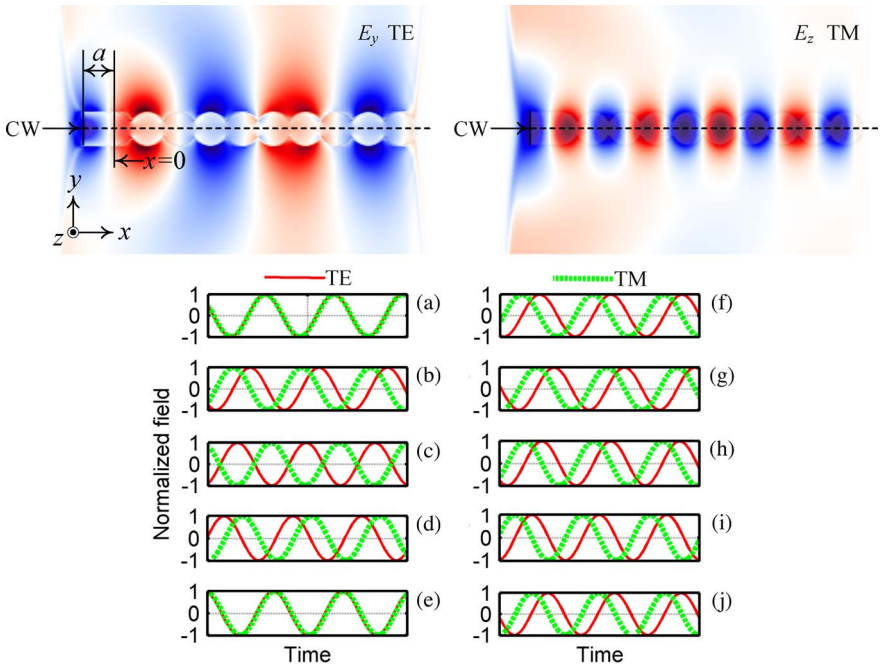

Fig. 5. (Top) Snapshots of the electric fields of TE (E_y) and TM (E_z) for PDW. (Bottom) Normalized electric fields of TE (E_y) and TM (E_z) at different locations and frequencies. The left column is $\omega = 0.145\ a/\lambda$ at different position. (a) $x = 3.4\ a$, (b) $x = 4.5\ a$, (c) $x = 5.55\ a$, (d) $x = 6.55\ a$, and (e) $x = 8.0\ a$. The right column is $x = 4.5\ a$ with different frequency. (f) $\omega = 0.140\ a/\lambda$, (g) $\omega = 0.142\ a/\lambda$, (h) $\omega = 0.145\ a/\lambda$, (i) $\omega = 0.148\ a/\lambda$, and (j) $\omega = 0.150\ a/\lambda$. The PDW is with $r = 0.55\ a$ and $\varepsilon = 12.96$.

influence of material dispersion to the birefringence and the phase difference of PDWs. The permittivity of Si is obtained by the following Sellmeier formula [27]:

$$\varepsilon = 11.6858 + \frac{0.939816}{\lambda^2} + \frac{0.000993358}{\lambda^2 - 1.22567}. \tag{1}$$

From the results above, we choose the radius of the Si rods as $0.55a$. Fig. 6(a) shows the birefringence (Δn) of the Si PDWs with different values of a. During the simulations, the indices of Silicon at different wavelength are obtained from (1). The birefringence increases with the increase of wavelength at the simulation window. However, the curves of phase difference $(\Delta\varphi)$ have different slopes, which can be seen in Fig. 6(b). Although the material dispersion can affect the birefringence of PDW, there is still wideband achromatic phase difference for the Si PDW. From the zoom-in pictures of phase difference shown in Fig. 6(c) and (d), we can see that larger than 100-nm bandwidth achromatic phase difference can be realized with the tolerance of $\pm 1^\circ$. By changing the length of lattice constant, the achromatic phase difference can be tuned to a different band. The bandwidth is affected by the length of PDW. Take $a = 240$ nm as an example. The values of $\Delta\varphi$ are $301 \pm 1^\circ$ at the band of 1495–1620 nm when $L = 4a$ and are $452 \pm 1^\circ$ at the band of 1506–1606 nm when $L = 6a$. The bandwidth of achromatic phase difference with same phase tolerance is narrower when the PDW is longer. The material dispersion does not strongly affect the phase difference of Si PDW.

5. High-Order WP Based on PDWs

The PDW is very suitable for the ultrahigh-order WP based on the formed birefringence [8] proposed previously by the authors. The key of the method is getting large propagation length

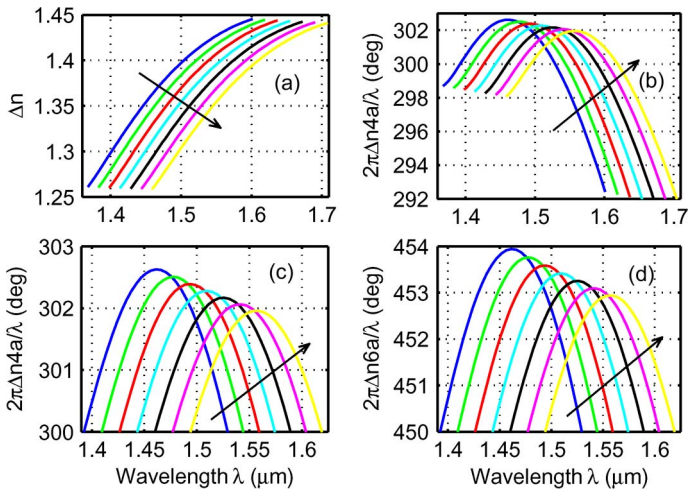

Fig. 6. (a) Birefringence (Δn) of Si PDWs. (b) Phase difference $(\Delta\varphi)$ of Si PDWs with $L = 4a$. (c) Zoom-in picture of $\Delta\varphi$ of Si PDW with $L = 4a$. (d) Zoom-in picture of $\Delta\varphi$ of Si PDW with $L = 6a$. The radius of the dielectric rod is $r = 0.55a$. Following the direction of arrows, the curves represent Δn or $\Delta\varphi$ of PDWs with different a of 225 nm, 227.5 nm, 230 nm, 232.5 nm, 235 nm, 237.5 nm, and 240 nm, respectively. The indices of Si are calculated by (1).

difference for the different polarizations, and the details will be found in [8]. To maximize the phase difference caused by path difference, we choose $\varepsilon = 9.6$ and $r = 0.5a$ (in this situation, the birefringence is achromatic at a broadband range). According to [8], the polarization beam splitter (PBS) and combiner (PBC) are the two essential elements for the formed birefringence structures. Here, we use directional couplers to realize the requisite PBS and PBC, and the details of the design procedure can be found in [23]. The distance between two rows of the directional coupler are chosen as $d = 2.8a$, as shown in Fig. 7(a). According to the dispersion curve [see Fig. 7(b)], which is obtained by PWM with a $1 \times 9a$ supercell [see Fig. 7(a)], the length of direct coupler is chosen, as $21a$ [see Fig. 7(c)]. To reduce the loss of the bend, a relatively large bend diameter $(11.48a)$ is chosen as shown in Fig. 7(c). The other parameters of the whole structure that combine the PBS and PBC can still be found in Fig. 7(c). The whole size of the simulation structure is about $240 \times 120a$. The power transmission spectrum that is shown in Fig. 7(e) is calculated by the 2-D FDTD simulation scheme. In the FDTD simulation procedure, the mesh size and time step are $\Delta x = \Delta y = 0.05a$ and $\Delta t = 0.5/(c\sqrt{(1/\Delta x)^2 + (1/\Delta y)^2})$. An adequately broadband Gaussian pulse is launched into the input port, and two linear detectors are placed in the input and output waveguide [as shown in Fig. 7(c)] to measure the time-varying electric and magnetic fields. The spectra are computed by taking the fast Fourier transform of the fields incorporating by integrating the Poynting vector over the cells of the detector lines. From the transmission spectrum, the transmission efficiencies are above 80% for both TE and TM in the frequency range of 0.18–$0.19a/\lambda$. The snapshots of the electromagnetic field (H_z for TE and E_z for TM) at the normalized frequency of $0.185a/\lambda$ for TE and TM polarization are shown in Fig. 7(c) and (d), respectively. From [8], the total phase difference can be written as $\Delta\varphi_{tol} = 2\pi\Delta nL_2/\lambda + 2\pi n_{TM}\Delta L/\lambda + \varphi_0$, and using the parameters of $\Delta n = 1.1505$, $L_2 = 240a$, $\Delta L = 980a$, $n_{TM} = 2.4427$, and $\omega = 0.185a/\lambda$, the phase difference caused by birefringence and formed birefringence are about 102π and 886π, respectively. Neglecting φ_0 (generally, it is a small value), the total phase difference is about 1000π, and it can serve as a 500th-order WP. It can depolarize a laser with full width at half maximum that is wider than 3.1 nm [28] and can be used in the depolarization of a Raman pump laser diode and super-luminescence LED used in the fiber gyro. Taking $\lambda = 1550$ nm as an example, the lattice constant a is about 287 nm. Therefore, the whole size of the 500th-order WP based on formed birefringence is about 69×34.5 μm.

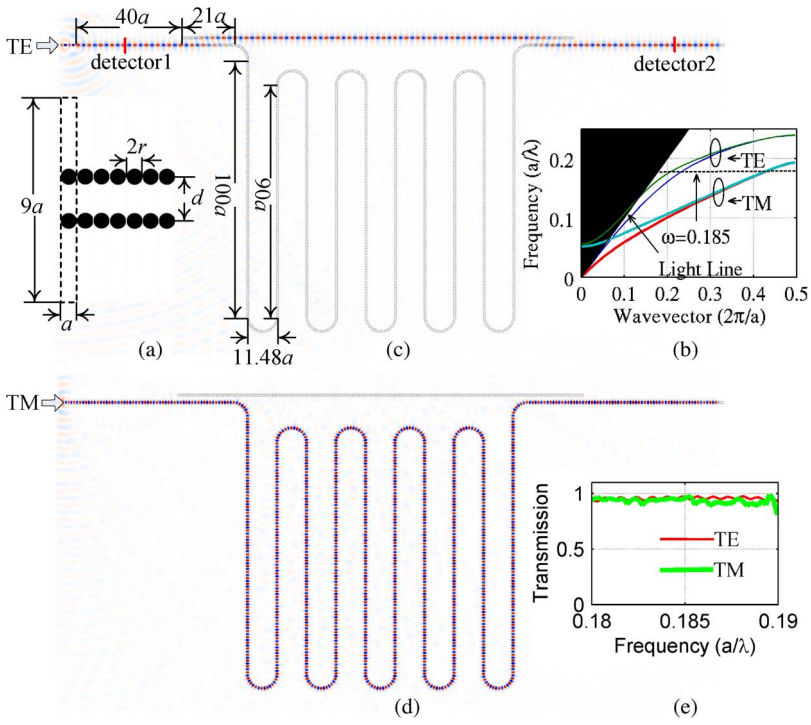

Fig. 7. High-order PDW WP based on formed birefringence. (a) Supercell structure of direct coupler (two rows PDW) used in PWM calculating. (b) Dispersion curve of the two rows PDW calculated by PWM using the supercell shown in (a). (c) and (d) Snapshots of the electromagnetic field distributions at the normalized frequency of 0.185 a/λ, for (c) TE (H_z) and (d) TM (E_z). (e) Power spectra of TE and TM polarizations [the input (detector 1) and output (detector 2) detectors are shown in (c)].

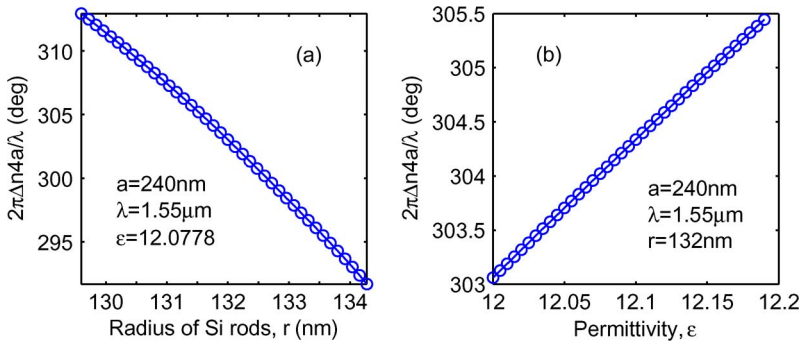

Fig. 8. Phase difference versus the small changing of (a) the radius of dielectric rods and (b) permittivity of the dielectric material.

6. Discussions and Conclusion

In practice, the fabrication tolerances should be considered first for that the physical sizes of the dielectric rods and the index of the material may be changed during the fabrication process. Here, we give a simple evaluation about the tolerance of phase difference with respect to the radius and the index of the dielectric rods. Take an Si-based PDW as example. The lattice constant and the operation wavelength are chosen as $a = 240$ nm and $\lambda = 1.55$ μm, respectively. The phase changing of $4a$ length Si PDW versus r and ϵ is shown in Fig. 8. From the figures, we can see that the phase difference has high tolerance with the material index but is sensitive to the radius of the dielectric rods. A little changing of the radius by 2 nm will give rise to more than 5° phase changing.

This is a challenge for practical fabrication. There are two methods that can be used to deal with this challenge: using the short length PDW to reduce the phase changing or adjusting the input and output conventional waveguides to compensate the phase changing.

Second, the loss of the PDW must be considered in practice, especially for high-order WP applications. There are four types of losses that should be taken into account: intrinsic loss of the PDW; coupling loss from the input and output coupling waveguides; out-of-plane loss, which is related to the vertical structure of the PDW; and the scattering loss by the roughness of nanorods in fabrication. The transmission characteristic of the high-order PDW shown in Fig. 7(b) is obtained by the 2-D FDTD method, and only intrinsic loss is considered. There are some additional losses that are missed, and more severe losses would be generated in practice. However, all the additional losses mentioned above can be well controlled by proper structure design and fine control in the fabrication process [29], [30]. A subwavelength grating periodic structure similar to PDW fabricated recently shows that the losses of both TE and TM polarization are less than 3 dB/cm for a bandwidth of 100 nm [29]. Actually, this value is small enough for high-order WP applications. Another aspect about the loss that must be indicated is that it is more important to control the TE and TM polarization having similar loss for some practical applications such as the polarization control [27]. Therefore, in practice, we should not only reduce the loss of PDWs but make the PDWs have the same attenuation for different polarizations as well.

In conclusion, we have demonstrated that PDWs with high index rods in air can have giant birefringence, which is higher than other all-dielectric structures such as MSDW $(\Delta n \sim 1)$ [5] and dielectric waveguide with angled slots $(\Delta n \sim 0.5)$ [31]. With proper design, both broadband (larger than 100 nm) achromatic birefringence and phase difference are obtained based on PDWs, even with material dispersion. Low-order broadband WP with high phase tolerance and ultracompact high-order WP are designed. The PDWs can be fabricated by the Electron beam lithography combining the inductively coupled plasma reactive ion etching method with the same as that used in [29] and [30]. The designed PDWs may find applications for polarization control in future photonic integrated circuits.

Acknowledgment

The authors wish to thank the anonymous reviewers for their valuable suggestions.

References

[1] M. F. Weber, C. A. Stover, L. R. Gilbert, T. J. Nevitt, and A. J. Ouderkirk, "Giant birefringent optics in multilayer polymer mirrors," *Science*, vol. 287, no. 5462, pp. 2451–2456, Mar. 2000.
[2] O. L. Muskens, M. T. Borgström, E. P. A. M. Bakkers, and J. Gómez Rivas, "Giant optical birefringence in ensembles of semiconductor nanowires," *Appl. Phys. Lett.*, vol. 89, no. 23, p. 233117, Dec. 2006.
[3] P. Weis, O. Paul, C. Imhof, R. Beigang, and M. Rahm, "Strongly birefringent metamaterials as negative index terahertz wave plates," *Appl. Phys. Lett.*, vol. 95, no. 17, p. 171104, Oct. 2009.
[4] S. Hsu, K. Lee, E. Lin, M. Lee, and P. Wei, "Giant birefringence induced by plasmonic nanoslit arrays," *Appl. Phys. Lett.*, vol. 95, no. 1, p. 013105, Jul. 2009.
[5] S. Yang, M. L. Cooper, P. R. Bandaru, and S. Mookherjea, "Giant birefringence in multi-slotted silicon nanophotonic waveguides," *Opt. Express*, vol. 16, no. 11, pp. 8306–8316, May 2008.
[6] F. Genereux, S. W. Leonard, and H. M. van Driel, "Large birefringence in two-dimensional silicon photonic crystals," *Phys. Rev. B, Condens. Matter*, vol. 63, no. 16, p. 161101, 2000.
[7] X. Xiao, B. Hou, W. Wen, and P. Sheng, "Tuning birefringence by using two-dimensional photonic band structure," *J. Appl. Phys.*, vol. 106, no. 8, p. 086103, Oct. 2009.
[8] W. Zhang, J. Liu, W. Huang, and W. Zhao, "Self-collimating photonic-crystal wave plates," *Opt. Lett.*, vol. 34, no. 17, pp. 2676–2678, Sep. 2009.
[9] S. Fan, J. N. Winn, A. Devenyi, J. C. Chen, R. D. Meade, and J. D. Joannopoulos, "Guided and defect modes in periodic dielectric waveguides," *J. Opt. Soc. Amer. B, Opt. Phys.*, vol. 12, no. 7, pp. 1267–1272, Jul. 1995.
[10] P. Luan and K. Chang, "Transmission characteristics of finite periodic dielectric waveguides," *Opt. Express*, vol. 14, no. 8, pp. 3263–3272, Apr. 2006.
[11] K. Lee, C. Chen, and Y. Lin, "Transmission characteristics of various bent periodic dielectric waveguides," *Opt. Quantum Electron.*, vol. 40, no. 9, pp. 633–643, Jul. 2008.
[12] D. N. Chigrin, A. V. Lavrinenko, and C. M. S. Torres, "Nanopillars photonic crystal waveguides," *Opt. Express*, vol. 12, no. 4, pp. 617–622, Feb. 2004.

[13] D. N. Chigrin, A. V. Lavrinenko, and C. M. S. Torres, "Numerical characterization of nanopillar photonic crystal waveguides and directional couplers," *Opt. Quantum Electron.*, vol. 37, no. 1–3, pp. 331–341, Jan. 2005.
[14] S. V. Zhukovsky, D. N. Chigrin, and J. Kroha, "Low-loss resonant modes in deterministically aperiodic nanopillar waveguides," *J. Opt. Soc. Amer. B, Opt. Phys.*, vol. 23, no. 10, pp. 2265–2272, Oct. 2006.
[15] D. N. Chigrin, S. V. Zhukovsky, A. V. Lavrinenko, and J. Kroha, "Coupled nanopillar waveguides optical properties and applications," *Phys. Stat. Sol. (A)*, vol. 204, no. 11, pp. 3647–3661, Nov. 2007.
[16] S. V. Zhukovsky, D. N. Chigrin, A. V. Lavrinenko, and J. Kroha, "Selective lasing in multimode periodic and non-periodic nanopillar waveguides," *Phys. Stat. Sol. (B)*, vol. 244, no. 4, pp. 1211–1218, Apr. 2007.
[17] Y. G. Boucher, A. V. Lavrinenko, and D. N. Chigrin, "Out-of-phase coupled periodic waveguides: A "couplonic" approach," *Opt. Quantum Electron.*, vol. 39, no. 10/11, pp. 837–847, Aug. 2007.
[18] A. A. Sukhorukov, A. V. Lavrinenko, D. N. Chigrin, D. E. Pelinovsky, and Y. S. Kivshar, "Slow-light dispersion in coupled periodic waveguides," *J. Opt. Soc. Amer. B, Opt. Phys.*, vol. 25, no. 12, pp. C65–C74, Dec. 2008.
[19] L. Dai, F. Wang, and C. Jiang, "Flatband slow wave in novel air-hole-array strip waveguides," *IEEE Photon. J.*, vol. 1, no. 3, pp. 178–183, Sep. 2009.
[20] Y. Zhang, W. Huang, and B. Li, "Fabry–Pérot microcavities with controllable resonant wavelengths in periodic dielectric waveguides," *Appl. Phys. Lett.*, vol. 93, no. 3, p. 031110, Jul. 2008.
[21] P. Luan and K. Chang, "Periodic dielectric waveguide beam splitter based on co-directional coupling," *Opt. Express*, vol. 15, no. 8, pp. 4536–4545, Apr. 2007.
[22] G. Zheng, H. Li, L. Jiang, W. Jia, H. Wang, and X. Li, "Design of an arbitrarily bent beam splitter for optical interconnections based on co-directional coupling mechanism," *J. Opt. A: Pure Appl. Opt.*, vol. 10, no. 12, p. 125303, Dec. 2008.
[23] W. Huang, Y. Zhang, and B. Li, "Ultracompact wavelength and polarization splitters in periodic dielectric waveguides," *Opt. Express*, vol. 16, no. 3, pp. 1600–1609, Feb. 2008.
[24] S. Zeng, Y. Zhang, and B. Li, "Self-imaging in periodic dielectric waveguides," *Opt. Express*, vol. 17, no. 1, pp. 365–378, Jan. 2009.
[25] S. G. Johnson and J. D. Joannopoulos, "Block-iterative frequency-domain methods for Maxwell's equations in a planewave basis," *Opt. Express*, vol. 8, no. 3, pp. 173–190, Jan. 2001.
[26] A. F. Oskooi, D. Roundy, M. Ibanescu, P. Bermel, J. D. Joannopoulos, and S. G. Johnson, "MEEP: A flexible free-software package for electromagnetic simulations by the FDTD method," *Comput. Phys. Commun.*, vol. 181, no. 3, pp. 687–702, Mar. 2010.
[27] L. Tong, J. Lou, and E. Mazur, "Single-mode guiding properties of subwavelength-diameter silica and silicon wire waveguides," *Opt. Express*, vol. 12, no. 6, pp. 1025–1035, Mar. 2004.
[28] N. Azami, E. Villeneuve, A. Villeneuve, and F. Gonthier, "All-SOP all-fibre depolariser," *Electron. Lett.*, vol. 39, no. 22, pp. 1573–1574, Oct. 2003.
[29] P. J. Bock, P. Cheben, J. H. Schmid, J. Lapointe, A. Delâge, S. Janz, G. C. Aers, D.-X. Xu, A. Densmore, and T. J. Hall, "Subwavelength grating periodic structures in silicon-on-insulator: A new type of microphotonic waveguide," *Opt. Express*, vol. 18, no. 19, pp. 20 251–20 262, Sep. 2010.
[30] P. J. Bock, P. Cheben, J. H. Schmid, J. Lapointe, A. Delâge, D.-X. Xu, S. Janz, A. Densmore, and T. J. Hall, "Subwavelength grating crossings for silicon wire waveguides," *Opt. Express*, vol. 18, no. 15, pp. 16 146–16 155, Jul. 2010.
[31] M. Kotlyar, L. Bolla, M. Midrio, L. O'Faolain, and T. Krauss, "Compact polarization converter in InP-based material," *Opt. Express*, vol. 13, no. 13, pp. 5040–5045, Jun. 2005.